Is Thermal Analysis Able to Provide Carbon and Silicon Contents of Cast Irons?

A. Regordosa, J. Lacaze, J. Sertucha, M. Castro-Roman, U. de La Torre, O. Dezellus

Is thermal analysis able to provide carbon and silicon contents of cast irons?

A. Regordosa[1], J. Lacaze[2], J. Sertucha[1], M.J. Castro-Roman[3], U. de la Torre[1], O. Dezellus[4]

1 Azterlan, Basque Research and Technology Alliance, Aliendalde Auzunea 6, E-48200 Durango (Bizkaia), Spain.

2. CIRIMAT, Université de Toulouse, CS 44362, 31030 Toulouse, France

3. Cinvestav Unidad Saltillo, Av. Industria Metalúrgica 1062, Parque Industrial Saltillo-Ramos Arizpe, Ramos Arizpe, Coahuila, Mexico, C.P. 25900.

4. LMI-UMR CNRS 5615 Université Lyon 1, 43 Bd du 11 novembre 1918, 69100 Villeurbanne, France

Abstract

The determination of silicon and carbon contents by thermal analysis is based on the recording of a cooling curve of a melt whose eutectic solidification takes place in the metastable system. The temperatures of the austenite and eutectic arrests are evaluated and then related to the carbon and silicon contents by linear relationships that would be defined by the phase diagram if there were no undercoolings. However, published experimental values of austenite liquidus arrest and metastable eutectic arrest both show significant undercoolings when compared to the equilibrium metastable Fe-C-Si phase diagram.

The undercooling of the austenite observed in hypo-eutectic alloys can be explained by tip undercooling during dendritic growth. On the other hand, it is pointed out that alloys with a composition close to stable eutectic - either slightly hypo- or slightly hypereutectic - can show much higher undercoolings than expected if stable eutectic precipitates. For such compositions, the thermal analysis could hardly be reproducible enough if the alloy does not solidify completely in the metastable system. Furthermore, the published experimental information on the temperature of the metastable eutectic is here supplemented by new results for silicon contents up to nearly 4 wt%. Both previous and new results show a similar undercooling of 5 to 15 °C compared to the calculated equilibrium metastable eutectic.

Each foundry wishing to use thermal analysis for carbon and silicon evaluation must determine its own relationships for austenite liquidus and metastable eutectic to account for the specificity of its melting process and casting system. Care should be taken to avoid any graphite precipitation in the thermal cup, and testing should be performed to improve reproducibility as this defines the accuracy of the composition determination.

Keywords: thermal analysis; cast iron; austenite liquidus; metastable eutectic; silicon content

Introduction

The basic principle of using thermal analysis (TA) to evaluate carbon and silicon contents in cast irons dates back to the 1960s and was presented in detailed works by Moore [1] and Heine [2]. The actual possibility of doing so is illustrated with Fig. 1-a that shows the isopleth Fe-C section at 2.0 wt.% Si of the Fe-C-Si phase diagram. In this figure, both the stable and metastable eutectics are shown at the intersection of the austenite liquidus with the graphite or cementite (Fe_3C) liquidus, respectively. By using 0.005-0.01 wt.% Bi [2] or about the same amount of Te as most often preferred, graphite growth is hindered, thus suppressing eutectic solidification in the stable system that then proceeds in the metastable system.

In this metastable system, "equilibrium" solidification of hypoeutectic alloys proceeds in two steps: i) precipitation of primary austenite starting at temperatures indicated as $T^{\gamma}_{L,1}$ and $T^{\gamma}_{L,2}$ for alloys #1 and #2, respectively; ii) solidification completion with the austenite-cementite eutectic processing at the same T_{EW} temperature for both alloys. The corresponding "equilibrium" TA records are schematically drawn in Fig. 1-b where the start of austenite precipitation is marked with a slope change while the eutectic corresponds to the plateau at T_{EW}.

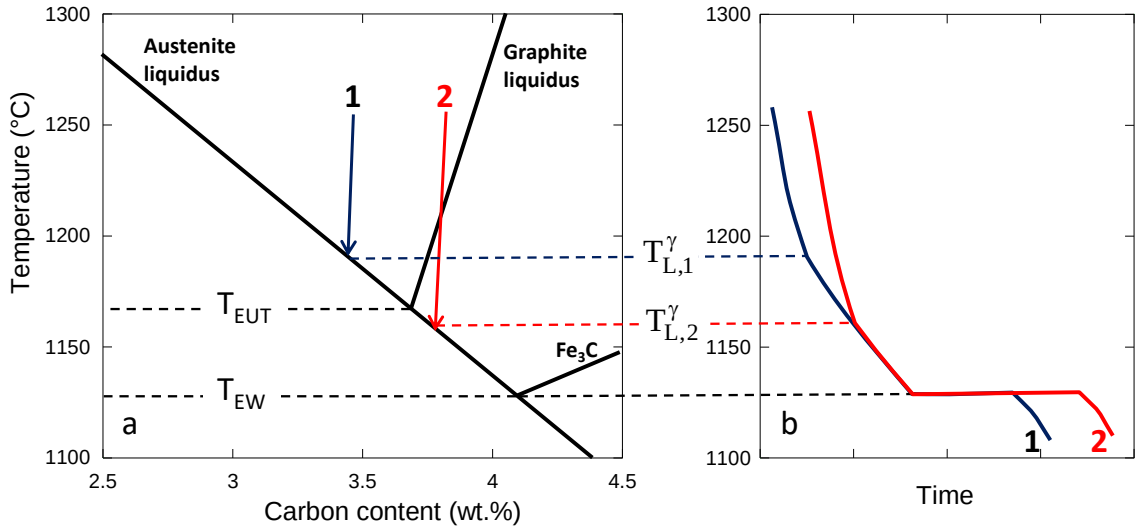

Figure 1. (a) Isopleth Fe-C section at 2 wt.% Si of the Fe-C-Si phase diagram showing both the stable eutectic at T_{EUT} and the metastable eutectic at T_{EW}. (b) Thermal records corresponding to "equilibrium" solidification in the metastable system of alloys #1 and #2 in (a).

The assumptions behind this "equilibrium" solidification in the metastable system are:

- There is no undercooling for nucleation AND growth of either primary austenite or austenite-cementite eutectic.

- There is no build-up of microsegregation in any element other than carbon so that solidification proceeds within the Fe-C isopleth section corresponding to the nominal composition of the alloy.

If these two assumptions are satisfied, then the knowledge of the phase diagram would give the characteristic temperatures of a given alloy. The inverse procedure, i.e. determining the composition from the characteristic temperatures read on a thermal record, usually assumes linear relationships between composition and austenite liquidus temperature. In the following, the analysis will be limited to the Fe-C-Si system for which the austenite liquidus T_L^γ is then expressed as:

$$T_L^\gamma = T_L^{\gamma,0} + m_C^\gamma \cdot w_C + m_{Si}^\gamma \cdot w_{Si} \qquad (1)$$

where $T_L^{\gamma,0}$ is a constant and m_i^γ is the liquidus slope relative to element i.

In the technical literature, Eq. (1) is most often written as:

$$T_L^\gamma = T_L^{\gamma,0} + m_C^\gamma \cdot \left(w_C + \frac{m_{Si}^\gamma}{m_C^\gamma} \cdot w_{Si} \right) = T_L^{\gamma,0} + m_C^\gamma \cdot CEL \qquad (1')$$

in which $CEL = \left(w_C + \frac{m_{Si}^\gamma}{m_C^\gamma} \cdot w_{Si} \right)$ is called the carbon equivalent austenite liquidus.

As an example and to give an order of magnitude, the following relation was determined based on phase diagram information [3, 4] for silicon content lower than 3 wt.%:

$$\mathrm{T_L^\gamma} = 1576.3 - 97.3 \cdot \mathrm{w_C} - 23.0 \cdot \mathrm{w_{Si}} = 1576.3 - 97.3 \cdot \left(\mathrm{w_C} + 0.236 \cdot \mathrm{w_{Si}} \right) \qquad (1'')$$

While the austenite liquidus relates to a surface in the Fe-C-Si diagram, the metastable eutectic is associated with a monovariant line. Accordingly, assuming again a simple linear relationship with composition gives:

$$T_{EW} = T_{EW}^0 + m_{Si}^W \cdot w_{Si} \qquad (2)$$

where T_{EW}^0 is the metastable eutectic temperature in the binary Fe-C phase diagram and is equal to 1148°C [5].

From Eq. (2), the silicon content of a cast iron considered as a Fe-C-Si alloy is thus simply given by:

$$w_{Si} = -\frac{T_{EW}^0 - T_{EW}}{m_{Si}^W} \qquad (3)$$

Inserting Eq. (3) in Eq. (1) and rearranging gives:

$$w_C = -\frac{T_L^{\gamma,0} - T_L^{\gamma}}{m_C^{\gamma}} + \frac{m_{Si}^{\gamma}}{m_C^{\gamma}} \cdot \frac{T_{EW}^{0} - T_{EW}}{m_{Si}^{W}} \qquad (4)$$

In summary, Eq. (3) and (4) demonstrate how straightforward should be the evaluation of the carbon and silicon contents of a Fe-C-Si alloy when the austenite liquidus and the metastable eutectic temperatures are known. However, in all practicality, this is far of being simple and in fact quite challenging for the foundries using this method because the two assumptions listed above are not fulfilled. Hence, the next two sections are devoted to detailing the consequences of undercooling of austenite and metastable eutectic transformations, respectively. In a final section are presented recent results on the metastable eutectic transformation of cast irons with silicon content up to 4 wt.%.

Austenite liquidus undercooling

Fig. 2 shows an example of an actual TA record with a marked arrest associated with austenite formation and a flat plateau corresponding to metastable eutectic. The austenite arrest is generally not recalescent and the characteristic T_{LA} temperature is most easily determined at the local maximum of the first dT/dt derivative as illustrated in the figure. Clearly, the actual temperature of the start of the austenite arrest – that is when the signal starts deviating from the liquid cooling slope (see the thick arrow) - is higher than the T_{LA} temperature as determined with the local maximum of the cooling rate. In other words, the austenite liquidus may well be underestimated when using the usual procedure for thermal analysis.

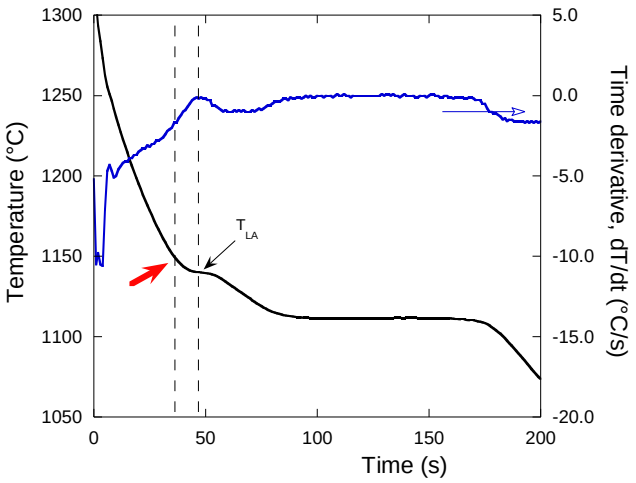

Figure 2. Example of TA record of a cast iron completing its solidification in the metastable system. The time derivative of the record (blue curve) is used to determine the T_{LA} temperature.

In fact, it has been shown that the austenite liquidus arrest also depends on a number of processing variables whose changes could lead to a scattering of T_{LA} of up to 10-15°C at a given CEL value [2, 6]. The use of TA for estimating the CEL is thus based on the hope that the scattering would be reduced at given melt processing conditions, i.e., in a given foundry plant. This means that any foundry using TA should carry out a campaign of trials at constant silicon content and variable carbon content so as to determine the coefficients T_{LA}^{0} and $m_C^{\gamma,\exp}$ of the experimental austenite liquidus that is expressed on the basis of Eq. (1') as:

$$T_{LA} = T_{LA}^{0} + m_C^{\gamma,exp} \cdot \left(w_C + \frac{m_{Si}^{\gamma,exp}}{m_C^{\gamma,exp}} \cdot w_{Si} \right) \qquad (5)$$

When the test campaign is conducted by varying the CEL values, the ratio $m_{Si}^{\gamma,exp} / m_C^{\gamma,exp}$ can be set to 0.25 as determined experimentally by Heine et al. [2] or to 0.236 as in equation (1''). Choosing either implies a difference in carbon content of 0.035 wt.% C at the same CEL value for alloys with 2.5 wt.% Si.

In the literature, there are a few series of T_{LA} temperatures at variable carbon content and constant silicon content. From the work by Moore [1], the values that are considered here relate to alloys with phosphorus content equal to or lower than 0.02 wt.% cast in both plain and tellurium coated molds. Two series with increasing carbon content are available in this work, at 1.0 wt.% Si (0.92 to 1.08 wt.% Si) and at 3.0 wt.% Si (2.82 to 3.03 wt.% Si). No significant effect of tellurium on T_{LA} was observed. The results are plotted in Fig. 3 with the dashed lines given by the best fit found by Moore, Eq. (5'):

$$T_{LA} = 1650 - 121 \cdot \left(w_C + 0.22 \cdot w_{Si} \right) \qquad (5')$$

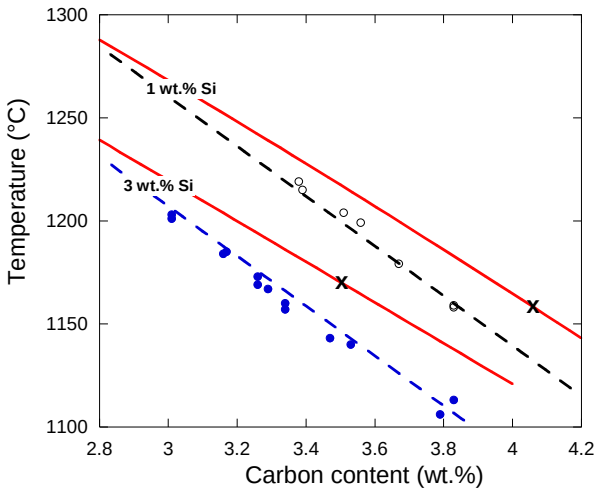

Figure 3. T_{LA} results from Moore [1] for alloys with 1 and 3 wt.% Si, P≤0.02wt.%. Dashed lines are according to Eq. (5') while solid lines represent the equilibrium austenite liquidus calculated with the TCFE-8 database. The cross along each of these solid lines locates the stable eutectic point.

It is worth noting that Moore reported also a good fit with the silicon coefficient at 0.25 as suggested by Heine [2]. The data in Fig. 3 are also compared to the liquidus calculated with Thermocalc software and the TCFE-8 database [7] that is shown with the solid line for both silicon contents. The cross on each calculated liquidus line corresponds to the equilibrium austenite-graphite eutectic. It is thus seen that the experimental austenite undercooling, i.e. the difference ($T_L^\gamma - T_{LA}$), is significant and increases with the carbon content. The same trend was observed with another series of data from Alagarsamy et al. [6] for lamellar grey irons with 2.26 wt.% Si (2.24-2.28 wt.% Si) and 0.7 wt.% Mn, as illustrated in Fig. 4. These experiments were carried out with plain and Te-coated cups and were also used to evaluate the experimental values of the metastable eutectic, $T_{EW}^{\exp}$, see next section. As before, the solid line in Fig. 4 represents the austenite liquidus calculated with the TCFE-8 database, and the cross locates the stable eutectic. The dotted line represents the fit through the experimental values while the dashed line labelled "calculated T_{LA}" is presented below.

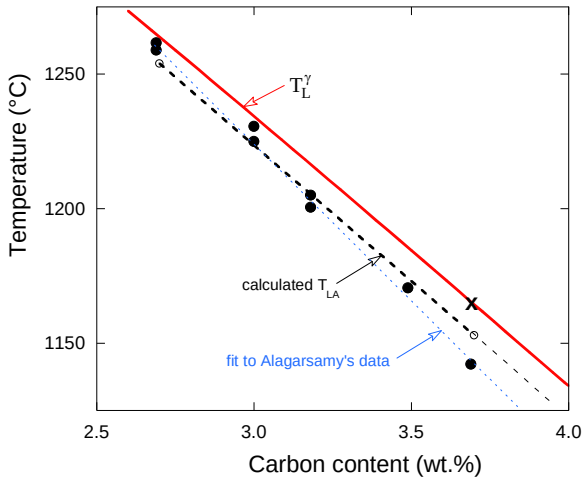

Figure 4. T_{LA} results from Alagarsamy et al. [6] for alloys with 2.26 wt.% Si and 0.7 wt.% Mn, with carbon content in the range 2.7 to 3.7 wt.%. The solid line shows the liquidus calculated with TCFE-8 and the cross locates the stable eutectic. The dotted line is a linear fit through the experimental values and the dashed line connects the two T_{LA} values calculated considering tip undercooling of austenite dendrites for 2.7 and 3.7 wt.% carbon (open discs); see text.

It is worth stressing that the austenite undercooling in the work of Moore (Fig. 3) appears systematically higher than in the work by Alagarsamy et al. (Fig. 4). It is unclear if this difference may be simply due to the way T_{LA} was determined or to differences in the melting and casting procedures [2, 6]. In practice, each series of data in Fig. 3 and Fig. 4 could be used to estimate values of T_{LA}^0 and $m_C^{\gamma,\exp}$ valid for the range of carbon content of interest as Moore did; see Eq. (5'). Specifically, the

differences in the T_{LA}-CEL correlation lines shown in Figures 3 and 4 confirm the need for each foundry to obtain the correlation equation that applies to their melting and casting procedures. With the correct equation, the dispersion of the T_{LA} data can be expected to be on the order of ±5°C to ±7.5°C [2]. Using this latter value, the error on the T_{LA} estimate will correspond to a dispersion of ±0.075 wt.% on the CEL value with a coefficient for carbon in the T_{LA} equation at about 100°C/wt.%.

On a more fundamental aspect, the increase of austenite undercooling with the carbon content seen in Fig. 3 and Fig. 4 is of interest. As austenite grows dendritically, it may be conjectured this is due in part to solute built up around the dendrite tips, whatever growth of austenite is columnar or equiaxed. Using an analysis for multicomponent alloys that has been already applied to Fe-C-Si alloys [8], it is shown in appendix A that this is effectively the case: the prominent effect is due to carbon build-up at the tip of the dendrites and the associated undercooling increases with the alloy's carbon content. An order of magnitude of austenite growth rate during solidification in TA cups is given by noticing it takes about 50 s for the T_{LA} arrest to show up in Fig. 2. As the distance from the surface to the center of a so-called square (SQ) cup is 17.5 mm (see Appendix B for the characteristics of the cups), this gives a growth rate average of 350 µm/s that is located with the vertical dashed line in Fig. A1. In these conditions, the undercooling at 3.7 wt.% carbon is 11.5°C, higher by about 2°C than the undercooling of 9.5°C at 2.7 wt.% carbon. The T_{LA} calculated from these two undercooling values have been reported in Fig. 4 (open discs) and connected with a dashed line denoted "calculated T_{LA}". It is seen to compare well with the set of experimental data (solid discs), except for the alloy at 3.7 wt.% C.

This trend of increasing austenite undercooling with the carbon content of hypoeutectic alloys could be observed also in Fig. 3 and, similarly, the same larger discrepancy for the highest carbon contents may be noticed for alloys that are near-eutectic (slightly hypo- or mildly hyper-eutectic) relative to the stable system. In fact, Alagasarmy et al. [6] reported that their sample for 3.7 wt.% carbon had a large grey rim. This strongly suggests that the experimental T_{LA} value for this alloy could well be associated with the growth temperature of the stable eutectic. More precisely, it is easy to consider that the solidification front consists of an array of austenite dendrites and of austenite/graphite eutectic proceeding together from the surface to the center of the TA cup. For hypoeutectic alloys, the dendrite tips will be ahead of the eutectic front, but as the nominal carbon content of the alloy is increased the distance between the two fronts will decrease and eventually cancel. This effect will be enhanced by austenite tip undercooling as schematized on the Fe-C isopleth section in Fig. 5 where the open circle shows the nominal carbon content of a slightly hypoeutectic alloy. The double arrow along the austenite liquidus illustrates the shift of the carbon content associated to the carbon build-up in the liquid at the dendrite tips. From the extremity of the double arrow, the horizontal arrow

relates the T_L^{γ} value for the tip composition to the T_{LA} value relative to the nominal carbon content. That the carbon content at and around the dendrite tips is well below the graphite liquidus makes it possible that the stable eutectic takes place close to the austenite dendrites solidification front. This situation depends on the actual growth temperature of the eutectic, whose possible variations are represented with the greyed area in Fig. 5. If the actual growth temperature of the eutectic is in the low part of this range, austenite dendrites may grow slightly ahead and a T_{LA} arrest may be recorded. On the contrary, if the eutectic growth temperature is at the upper limit of the greyed zone, the austenite dendrites will eventually be engulfed by the eutectic front before reaching the cup's center, and only a eutectic arrest will be detected.

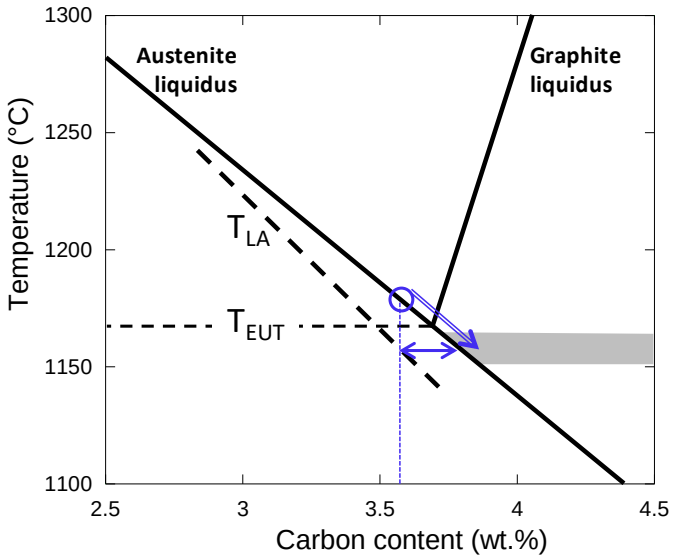

Figure 5. Fe-C isopleth at 2 wt.% Si showing the shift to higher carbon content in the liquid at the dendrite tips (double arrow) and its relation to austenite undercooling (horizontal arrow).The nominal carbon content of the considered alloy is represented with the open circle. The greyed area shows a range of possible eutectic growth temperatures.

The above description explains why the T_{LA} arrest sometimes disappears in near-eutectic alloys as pointed out a long time ago by Chaudhari et al. [9, 10]. Fig. 5 illustrates a further practical consequence of austenite undercooling when considering again the slightly hypoeutectic alloy represented with the open disc. In the case the alloy is conveniently inoculated, the stable eutectic may proceed at a temperature similar or slightly higher than that at which austenite dendrites would grow accounting for tip undercooling. In such a case, there will be no T_{LA} arrest recorded during TA analysis and the alloy will be considered as eutectic. The schematic in Fig. 5 shows that it will lead to an apparent eutectic composition that is lower than the true stable eutectic composition. In other words, there is a shift of the apparent eutectic composition to lower carbon content that might explain why the carbon equivalent of the eutectic is most often set at 4.26 wt.% while the assessed

phase diagram value is 4.34 wt.% [5]. Finally, it should be mentioned that the shaded area in Figure 5 will be located at higher undercoolings with respect to the stable eutectic temperature for spheroidal graphite irons than for lamellar graphite irons, thus leading to an apparent eutectic composition at a higher CE content for the former than for the latter.

Metastable eutectic arrest

Heine [2] reported a large number of results on metastable solidification that were obtained by thermal analysis using cups of different sizes. Metastable solidification is characterized by a nearly flat eutectic plateau with or without recalescence, leading Heine to report both minimum and maximum temperatures. In some cases, recalescence was associated with mottling and sometimes not. In the table 4 of Heine's paper, it can be seen that recalescence could go up to 6°C for a eutectic microstructure given as fully metastable (white). However, in most of the cases, no indication was given about the microstructure, so that it appears difficult to use these data. Furthermore, Heine found that an upper limit for the metastable eutectic arrest could be expressed as (°C):

$$T_{EW} = 1154.3 - 20.2 \cdot w_{Si} - 48.6 \cdot w_P \qquad (6)$$

It is noticeable that the value of 1154.3 corresponds quite exactly to the stable binary Fe-C eutectic and not to the metastable one at 1148°C, thus raising some doubt on this equation.

Because of the use of thermal cups with various sizes, Heine [2] noticed a high scattering of up to 30°C at given silicon content that can be firstly due to the effect of varying cooling rate. Indeed, the growth law of the metastable austenite-Fe_3C eutectic can be expressed as $V=\alpha\cdot(\Delta T_{EW})^2$, where V is the growth rate and ΔT_{EW} the undercooling with respect to T_{EW}. The coefficient α has value of a few tens of $\mu m\cdot s^{-1}\cdot °C^{-2}$ [11, 12]. Such a growth law results in an undercooling that increases with the cooling rate in small castings as demonstrated by Oldfield and Humphreys [13] who cast alloys in cylinders of various sizes leading to a large range of cooling rates. Every cylinder was equipped with a thermocouple for thermal analysis and the microstructure was observed. Available results from Oldfield and Humphreys [13] on 4 taps of a Fe-C-2%Si alloy and Miyake and Okada [14] on small castings of an Fe-3.3%C alloy are shown in Fig. 6. The plot confirms a significant sensitivity of the eutectic thermal arrest to cooling rate. For phase diagram determination, it is usual practice to consider that the relevant value is obtained by extrapolating the results to a zero cooling rate, which gave 1123°C for the Oldfield and Humphreys data at 2 wt.% silicon.

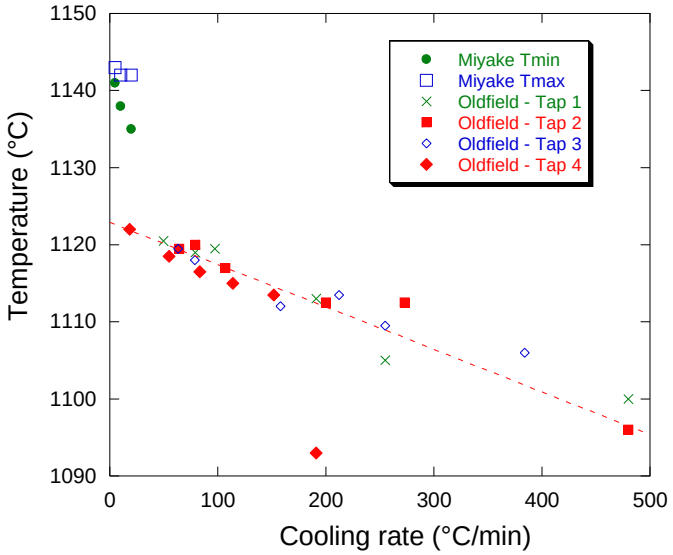

Figure 6. Effect of cooling rate on the temperature of the metastable eutectic as measured by Miyake and Okada on Fe-3.3C alloy [14] and Oldfield and Humphreys for 2 wt.% Si [13]. The line is a guide through the data by Oldfield and Humphreys [13] that extrapolates to 1123°C.

This extrapolation was systematically done by Oldfield [15] on a series of alloys with 0 or 0.5 wt.% Mn, 0 to 0.1 wt.% Cr, and Si content up to 2 wt.%. For the higher silicon contents, the author indicated that the extrapolation was not easy because several cylinders showed a mottled structure, so that both minimum and maximum estimates were reported by Oldfield (his table 3). Various attempts were made to use this data and it was found convenient to consider the minimum temperature. These values were thus reported with solid discs as a function of the silicon content in Fig. 7 where a large scattering is seen. However, a line extrapolating to the binary metastable eutectic temperature of 1148°C can easily be drawn by putting more weight on the highest values as illustrated with the upper line in Fig. 7 that writes:

$$T_{EW}=1148-12.23\cdot w_{Si} \qquad (7)$$

A number of results from TA analysis with Te-bearing cups are available which have been reported also on the graph in Fig. 7. These results are mostly from Heine [16, 17] with some from melts containing 0.46-0.81 wt.% Mn that are represented with open symbols while solid symbols are for melts with no or little (<0.2 wt.%) Mn. There is no clear effect of Mn that is seen to change the temperature in both directions (positive and negative), in agreement with the very small effect assessed by Kanno [18]. Other results are from Moore [1], for which only data for alloys with less than 0.02 wt.% P were selected. Also, two values from Cree et al. [19] for an industrial SGI cast in two different cups (so called round, RD, and square, SQ, see Appendix B for the characteristics of the cups) are shown. Finally, the average of the values reported by Alagarsamy et al. [6], namely 1114°C, was considered.

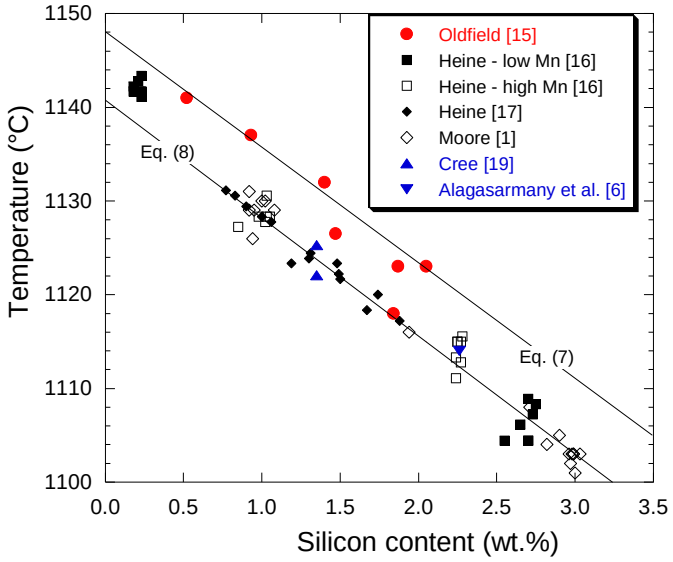

Figure 7. Effect of silicon on the temperature of the metastable eutectic. The data from Oldfield have been obtained by extrapolating records at various cooling rates. All other results are from TA analysis in Te-bearing cups.

It is noted that all TA values in Fig. 7 are below those of Oldfield by an amount that seems not to depend on silicon content. For further discussion, the metastable temperature measured with TA cup will be denoted T_{EW}^{cup}. The line going through these results in Fig. 7 corresponds to the equation given by Heine for Te-coated cups [17] and expressed as:

$$T_{EW}^{cup} = 1140.8 - 12.6 \cdot w_{Si} \qquad (8)$$

The line corresponding to Eq. (8) nearly parallels the one from Eq. (7) with a downward shift of about 7°C. Kanno et al. [18] have offered an equation giving the metastable temperature as a function of alloying content for several elements of interest. Limited to silicon, the equation is:

$$\mathrm{TEC} = 1142.6 - 11.6 \cdot \mathrm{w_{Si}} \qquad (9)$$

Eq. (9) gives a line located in between the two lines in Fig. 7.

While Eq. (7) relates to the "equilibrium" value of the metastable eutectic, Eq. (8) is the reference equation for estimating silicon content by thermal analysis, i.e., at finite cooling rate. The scatter of the TA data in Fig. 7 is in part due to the use of different TA cups as exemplified by the SQ and RD results from Cree et al. [19]. However, even for a given cup, the scatter is noticeable, being about 6°C for RD cup and 8°C for SQ cup according to Cree et al. Such a range agrees with the scatter of 5°C that can be seen in the data by Alagasarmany et al. [6]. Using the slope in Eq. (8), a scatter of 5°C (±2.5°C) corresponds to a possible error of ±0.2 wt.% Si.

A final note should be made about the fact that for silicon contents higher than 4 to 5 wt.% a ternary silico-carbide appears as evidenced by a number of authors amongst whom Faivre et al. [20]. These authors identified it as Marles' carbide but other structures have been reported. The important consequence for the present study is that above this silicon content the two phase austenite/cementite eutectic will be replaced by a three phase austenite/cementite/silico-carbide eutectic. Such a three phase eutectic will be an invariant in the ternary Fe-C-Si system, meaning that the eutectic arrest will occur at a constant temperature for silicon content higher than the critical limit.

Analysis of recent data

A non-inoculated melt that was prepared for casting SGI was then maintained during 8 hours in a pressurized unit as described with full details for a previous series of trials [4]. Every 20-25 minutes, a medal for chemical analysis and a set of SQ and RD TA cups were cast, of which the RD plain one was selected. Fig. 8 shows the evolution during holding of the content in C, Si and spheroidizing elements (Mg, Ce and La) of the melt that contained also 0.56 Mn and 0.14 Cu (wt.%). The carbon content remained nearly constant until the last four samples when it showed a decrease by about 0.1 wt.%. The silicon content could be considered as constant at an average value of 2.42 wt.%. As expected, the amount of the three spheroidizing elements decreased significantly all along the melt holding.

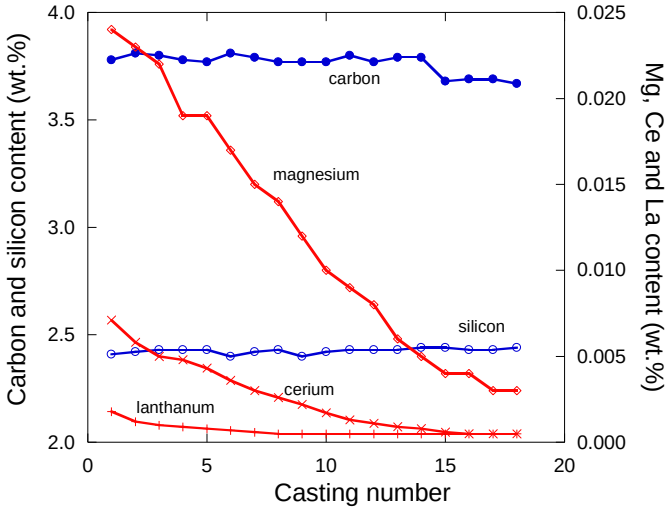

Figure 8. Evolution of the composition during the 8 hours holding.

Fig. 9 shows the whole set of TA records over the 8 hours holding, with the curves shifted from left to right according to the indicated time of pouring. The first two records show a recalescent eutectic reaction whose shape can definitely be associated with solidification of the stable graphitic eutectic.

On the contrary, all subsequent cooling curves showed a flat plateau at a temperature slightly higher than 1110°C with sometimes limited recalescence, demonstrating a mostly metastable white eutectic solidification took place. This evolution between the first two and later records indicates that some nuclei for graphite precipitation were present at the beginning of the melt holding, which then disappeared together with fading of spheroidizing elements [4].

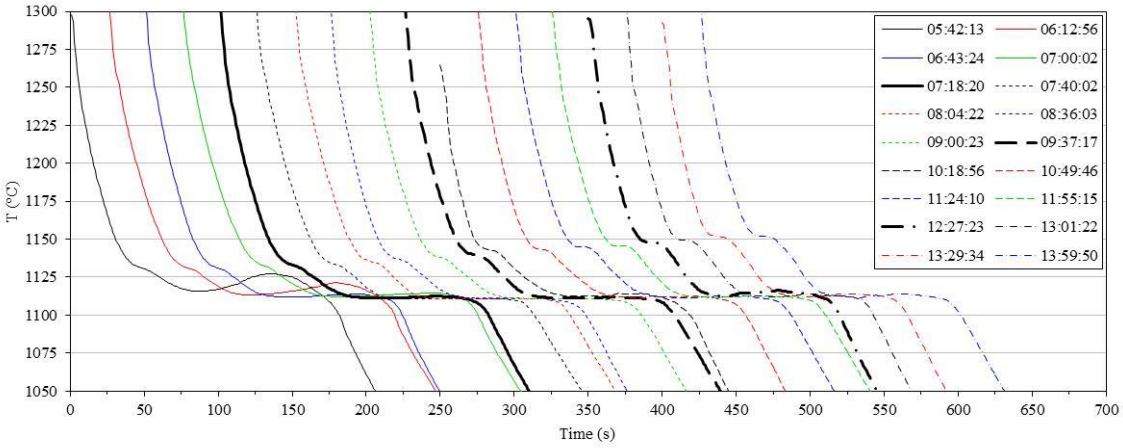

Figure 9. Whole set of cooling curves with plain RD TA cups. The curves have been shifted along the X axis for clarity.

The eutectic plateau has been characterized by the minimum and maximum temperatures, excluding the first two records that did not show a flat plateau. The results are plotted in Fig. 10 with solid symbols for the minimum temperature, $T_{e,min}$, and open symbols for the maximum temperature, $T_{e,max}$. On the graph are also shown with grey horizontal lines the T_{EW} and T_{EW}^{cup} temperatures calculated with eq. (7) and (8), respectively. The width of these lines was set so as to indicate the maximum change of these temperatures due to silicon evolution during holding. It is seen that all $T_{e,min}$ values are in the range [T_{EW}^{cup} , T_{EW}^{cup} +2°C], well below T_{EW}. Because of the expected accuracy of the measurements with the TA cups, which can be estimated to be ±2.5°C at 1100°C see Appendix B), the $T_{e,min}$ values can be considered fairly reproducible. This high reproducibility is encouraging, but it should be noted that the thermocouples used in this work could well have been part of the same batch, i.e. having the same bias. For analyses that would be performed over a longer period of time, it may be useful to consider the possibility of higher biases and therefore to expect larger errors.

The results in Fig. 10 have been replotted in Fig. 11 as $T_{e,min}$ (solid symbols) and recalescence (open symbols) versus casting number, with an enlarged scale. Recalescence is a relative value that does not depend on thermocouple's accuracy and it is thus of interest to note that it can vary in between near zero and 4°C. These non-zero values can be related either to the appearance of a white eutectic

cell close to the thermocouple junction, or to the competitive growth of some graphite/austenite eutectic cells during a transformation proceeding mostly in the metastable system [21]. It can be considered that a recalescence value higher than 5°C would be a clear indication of growth of several stable eutectic cells whose presence may affect also the $T_{e,min}$ value. In summary, provided that recalescence is lower than 5°C, the characteristic temperature of the metastable transformation is properly estimated by $T_{e,min}$, though this estimate may be slightly biased by excess.

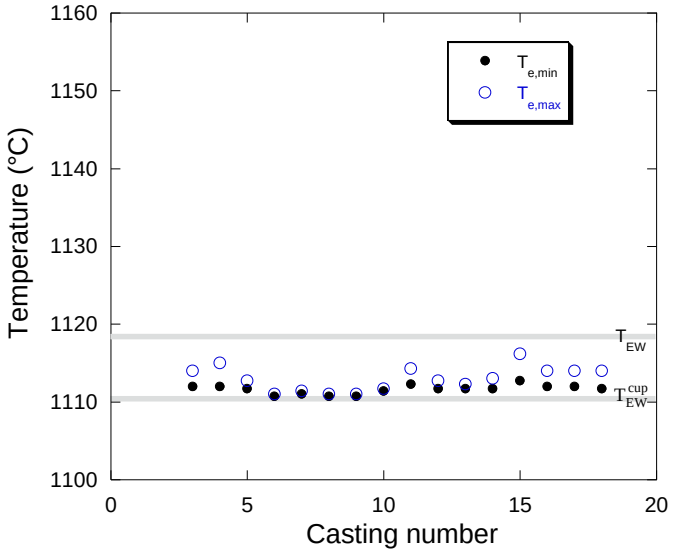

Figure 10. Results for plain RD cups. The horizontal grey lines have a width representative of the maximum range of variation of T_{EW} and T_{EW}^{cup} according to the indicated range of silicon content.

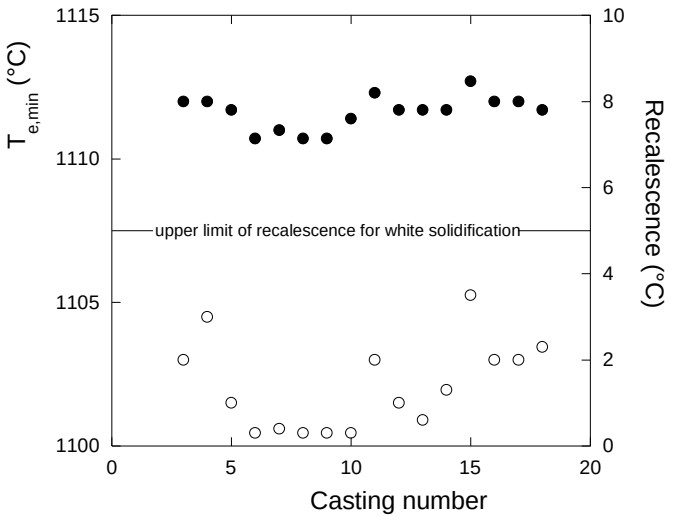

Figure 11. Results shown in Fig. 10 replotted as $T_{e,min}$ (solid symbols) and recalescence (open symbols). The horizontal line suggests a maximum allowable recalescence value of 5°C for transformation in the metastable system.

Three other similar series of castings of a melt maintained in a pressurized pouring unit have been carried out during these last two years. In all of them, plain SQ TA cups were available whose results are presented in Appendix B. The average $T_{e,min}$ values related to the metastable eutectic of these three series and that of data in Fig. 11 are reported in Fig. 12 where they are complemented with results from Alagarsamy et al. and Cree et al. who used similarly sized TA cups. Finally, a series of TA records of cast irons with silicon content varying from 2.2 to 3.9 wt.% was gathered from experiments carried out during the last decade at the TQC foundry. They were all obtained with SQ cups, and are presented in Appendix C and also reported in Fig. 12.

Figure 12 shows that the previous results and the new results for silicon content between 2.5 and 3 wt% are in reasonable agreement with each other. However, most importantly, there is a significant decrease in the metastable eutectic temperature for silicon contents above 3 wt%. This curvature of T_{EW}^{cup} with silicon content is in agreement with the T_{EW} curve calculated with TCFE-8 and represented by the solid line in Fig. 12. For silicon contents above 4.5 wt%, the horizontal solid line indicates that the three-phase eutectic was reached at about 1074.4°C. Unfortunately, no experimental data for such high silicon contents seem to exist for unalloyed cast irons.

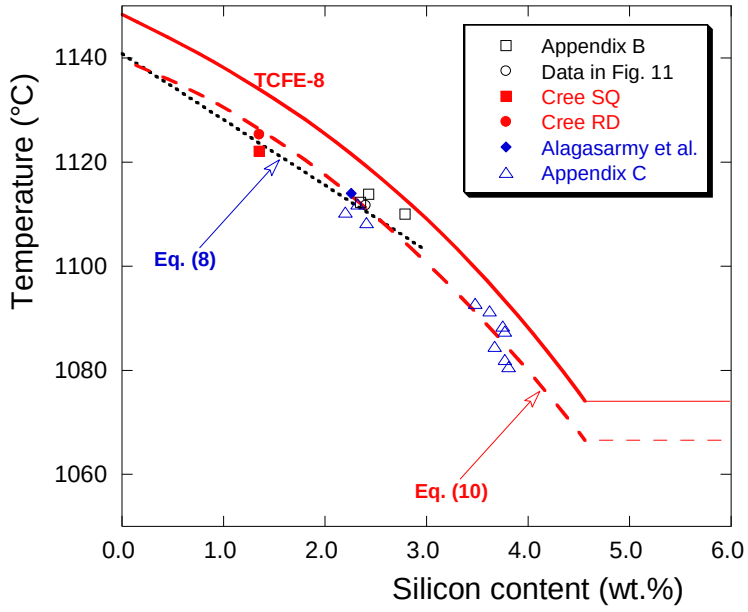

Figure 12. Effect of silicon content on the $T_{e,min}$ value as measured on standard RD and SQ TA cups. The dotted line was drawn according to Eq. (8) and the dashed curve according to Eq. (10).

The curve calculated with TCFE-8 has been fitted with a second order polynomial and then shifted downwards by 8°C. The corresponding equation represents T_{EW}^{cup} for silicon contents up to 4.5 wt.% and is written:

$$T_{EW}^{cup} = 1139.6 - 7.16 \cdot w_{Si} - 1.94 \cdot w_{Si}^2 \qquad (10)$$

Eq. (10) has been represented with a dashed curve in Fig. 12 and complemented with an horizontal line at 1066.4°C for silicon contents higher than 4.5 wt.%. For Si content up to 4.5 wt.%, Eq. (10) can be reverted to give the silicon content as function of $T_{e,min}$:

$$w_{Si} = 0.718 \cdot \sqrt{1147.04 - T_{e,min}} - 1.845 \qquad (11)$$

The value of T_{EW}^{cup} given by Eq. (8) is also shown with the dotted line in Fig. 12. It appears possible to use it for silicon content lower than 3 wt.% though the use of Eq. (11) would be more consistent. According to Eq. (8), knowing $T_{e,min}$ at ±2.5°C converts to a possible precision on silicon estimate of ±0.2 wt.% that is quite large though maybe also optimistic.

Conclusion

Based on the knowledge of the Fe-C-Si phase diagram, the undercooling of primary dendritic austenite has been evidenced and can be calculated for a particular TA cup. This undercooling depends mostly on the size and shape of the TA cup and increases slightly with the carbon content for hypoeutectic alloys. With these results, the very high undercoolings sometimes experienced by austenite when the alloy is near eutectic, either slightly hypo- or mildly hypereutectic, has been analyzed as resulting from a coupling between dendritic growth of austenite and growth of stable eutectic, even when this latter is limited to a rim at the outer surface of the TA cup. These conclusions are very much in line with previous observations on mildly and strongly hypereutectic alloys [22], confirming that TA records on near eutectic alloys may give confusing results. This analysis also suggests why the often used eutectic carbon equivalent of 4.26 wt.% is lower than the assessed value at 4.34 wt.%.

The above analysis implies that graphite growth should be totally hindered if correct T_{LA} values are to be evaluated on alloys that are near eutectic and mildly hypereutectic in the stable system. If this is effectively achieved, then every foundry could characterize its own thermal analysis process and provide its own linear equation relating T_{LA} and CEL. A reasonable scattering of ±5.0°C [2] on the T_{LA} estimate will correspond to a dispersion of about ±0.05 wt.% on the CEL value. If at the same time

sufficient care is allowed in analyzing the metastable eutectic reaction, one could expect to determine the silicon content with an accuracy of about ±0.2 wt.%.

References

[1] A. Moore, Carbon equivalent of white cast irons, AFS Cast Metals Research J., March 15 (1972)

[2] R.W. Heine, Liquidus and eutectic temperatures and solidification of white cast irons, AFS Trans. 85, 537 (1977)

[3] M. Castro, M. Herrera, M.M. Cisneros, G. Lesoult, J. Lacaze, Simulation of thermal analysis applied to the description of the solidification of hypereutectic SG cast irons"; Int. J. Cast Metals Research 11, 369 (1999)

[4] A. Regordosa, U. de la Torre, J. Sertucha, J. Lacaze, Quantitative analysis of the effect of inoculation and magnesium content on compacted graphite irons – Experimental approach, J. Materials Processing and Technology 9, 11332 (2020)

[5] P. Gustafsson, Assessment of the Fe-C phase diagram, *Scand. J. Metall.* 14, 259 (1985)

[6] A. Alagarsamy, F.W. Jacobs, G.R. Strong, R.W. Heine, Carbon equivalent vs. austenite liquidus: what is the correct relationship for cast irons?, AFS Trans. 92, 871 (1984)

[7] Thermocalc softwares and databases, https://thermocalc.com/products/

[8] N. Siredey, J. Lacaze, Growth conditions at the solidification front of multicomponent alloys, Scripta Metallurgica et Materialia 29, 759 (1993)

[9] M.D. Chaudhari, R.W. Heine and C.R. Loper, Potential Applications of cooling curves in ductile iron process control, *AFS Trans.* 82, 379 (1974)

[10] M.D. Chaudhari, R.W. Heine and C.R. Loper, Principles involved in the use of cooling curves in ductile iron process control, *AFS Cast Metals Res. J.* 11, 52 (1975)

[11] H. Jones, W. Kurz, Relation of interphase spacing and growth temperature to growth velocity in Fe-C and Fe-Fe_3C eutectic alloys, Z. Metallkde. 72, 792 (1981)

[12] M. Hillert, V.V. Subba Rao, Grey and white solidification of cast iron, ISI Publ. 110, The Iron and Steel Institute, 1968, pp. 204-212

[13] W. Oldfield, J.G. Humphreys, Formation of nodular graphite in hypo-eutectic irons, BCIRA J. 10, 315 (1962)

[14] H. Miyake, A. Okada, Nucleation and growth of primary austenite in hypoeutectic cast iron, AFS Trans. 106, 581 (1998)

[15] W. Oldfield, The chill-reducing mechanism of silicon in cast iron, BCIRA J. 10, 17 (1962)

[16] R.W. Heine, The Fe-C-Si solidification diagram for cast irons, AFS Trans. 94, 391 (1986)

[17] R.W. Heine, Austenite liquidus, carbide eutectic and undercooling in process control of ductile base iron, AFS Trans. 103, 199 (1995)

[18] T. Kanno, Y. Iwami, I. Kang, Prediction of graphite nodule count and shrinkage tendency in ductile cast iron, with 1 cup thermal analysis, Int. J. Metalcasting 11, 94 (2017)

[19] J. Cree, I. Grybush, M. Robles, et al., Statistical Comparisons of Four (4) Different Thermal Analysis Sample Cup Types for Chemistry Control of Ductile Base Iron, International Journal of Metalcasting 15, 729 (2021)

[20] R. Faivre, B. Vigneron, M. Degois, Influence de la teneur en carbone et en silicium sur la formation et la morphologie du graphite dans les alliages fer-carbone-silicium de type fonte, Hommes et Fonderie, Mars 1972, pp. 13-25

[21] J. Lacaze, A. Regordosa, J. Sertucha, U. de la Torre, Quantitative analysis of solidification of compacted graphite irons – A modelling approach, ISIJ International 61, 1539 (2021)-1549

[22] M. J. Castro-Román, J. Lacaze, A. Regordosa, J. Sertucha, R. del Campo-Castro, Revisiting Thermal Analysis of Hypereutectic Spheroidal Graphite Cast Irons, Metall. Mater. Trans. 51A, 6373 (2020)

[23] M. Bobadilla, J. Lacaze, G. Lesoult, Influence des conditions de solidification sur le déroulement de la solidification des aciers inoxydables austénitiques, J. Crystal Growth 89, 531 (1988)

Appendix A. Growth undercooling of austenite dendrites

Growth of austenite in hypoeutectic cast irons is dendritic and proceeds with some undercooling due to redistribution of solutes at the dendrite tips. An approximate solution for multicomponent alloys has been derived previously and applied to ternary Fe-Ni-Cr [23] and Fe-C-Si alloys [8], showing in both cases a good agreement with experimental information. In this model, the tip radius is calculated as a function of the growth rate using the marginal stability criterion, considering the tip to be a paraboloid. In the case of a slightly hypoeutectic Fe-C-Si alloy, it was found that accounting for silicon has little effect. Accordingly, the present calculations were limited to binary Fe-C alloys with the aim of comparing the tip undercooling of two alloys at 2.7 and 3.7 wt.% carbon as being representative of the extreme compositions investigated by Alagarsamy et al. [6]. For alloys with 2 wt.% silicon, calculations using the TCFE-8 database gave a partition coefficient for carbon of 0.42 and a liquidus slope relative to carbon of -100°C/wt.% that were used for calculations. With other parameters set as before [8], the calculated change in tip undercooling with growth rate is shown in Fig. A1 (note that no consideration was taken of plane front and cellular growth at growth rates lower than about 1 µm/s). Based on the size of the TA cups and on the time for the T_{LA} temperature to be reached (50 s in Fig. 2 and 9), a typical growth rate of austenite from the surface to the centre of the cups is 350 µm/s. For this growth rate, Fig. A1 shows that austenite undercooling is of the order of 10°C. It is also clearly seen that the tip undercooling for growth of austenite is larger for an alloy at 3.7 wt.% carbon than for an alloy with 2.7 wt.% carbon.

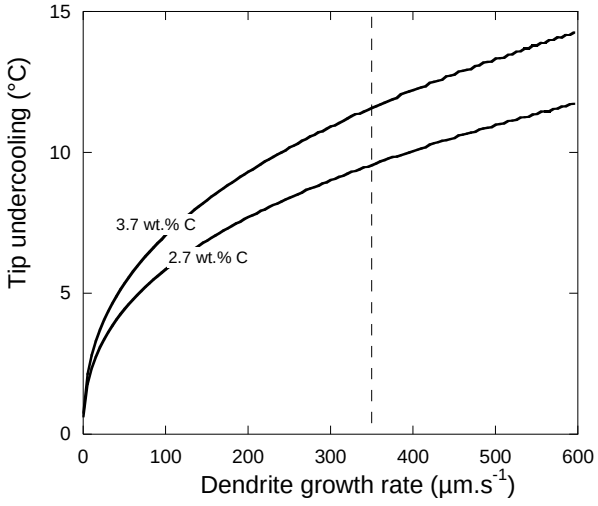

Figure A1. Calculated tip undercooling of dendritic austenite for Fe-C alloys with 2.7 and 3.7 wt.% carbon.

The above calculations demonstrate the role of carbon on the undercooling at the front of dendritic austenite. As noticed above, the effect of silicon is limited, this is because its partition coefficient is close to 1, and it has been verified that elements such as sulfur or oxygen that have small partition coefficient have also little effect because their content is low.

Appendix B – Metastable eutectic temperatures in series with melt hold in a press-pour furnace.

Several series of trials have been carried out in the same conditions as depicted in the main text: a melt prepared for casting SGI parts was held for hours in a pressurized unit so as to have a slow fading of spheroidizing elements. Every 20-25 minutes, various TA cups were cast as well as a medal for chemical analysis.

Amongst the available data, those related to plain cups were selected, which all were SQ cups for the data shown in this appendix while those in the main text were RD cups. The SQ and RD cups are from Heraeus Electro-Nite with SQ cups having a conical parallelepiped shape with a bottom base 35x35 mm, a upper base 37x37 mm and a height of 40 mm. The RD cups define a cylindrical volume with 34 mm in diameter and 40 mm in height.

The accuracy of the temperature measurements depends on the cups, on the one hand, and on the recording system, on the other hand. Concerning the cups, the supplier reports an accuracy of $\pm$1.1ºC at 1000ºC. On the other hand, the system consisting of the temperature recorder, the connecting wires and the plug-holder are calibrated before each series of experiments and checked to obtain an average accuracy of $\pm$0.4ºC at 1050ºC and of $\pm$0.5ºC at 1210ºC. Combining the accuracy value at 1000ºC for the cup and that at 1050°C for the recording system, a combined value of $\pm$1.2ºC is obtained for the whole measuring system in the temperature range 1000-1050°C. As the accuracy decreases with temperature, the expected accuracy of the whole measurement system was estimated to ±2.5°C for the range between 1100°C and 1200°C.

Fig. B1-B3 show the $T_{e,min}$ (solid symbols) and recalescence (open symbols) values for each of these series. It has been considered that the eutectic plateau of a TA record relates to metastable solidification provided $T_{e,min}$ is lower than 1125°C and recalescence is at maximum 5°C. These critical values have been selected based on previous and present experiences. The shaded areas in Figs. B1-B3 have been drawn using the recalescence cut-off value and are intended to facilitate the visualisation of the relevant results.

Table B-1. Reference of the experimental series, range of silicon content (%Si) and of recorded $T_{e,min}$ values.

Series reference	%Si (wt.%)	$T_{e,min}$ (°C)
1	2.39-2.45	1111.1-1116.4
2	2.33-2.37	1111.0-1113.5
4	2.76-2.82	1107.8-1112.2

In Fig. B1 and B2 is observed a certain tendency for recalescence to decrease with casting number, i.e., with time of holding of the melt. This could be indicative that some stable eutectic cells developed together with the metastable eutectic cells, in a number that decreased with holding time [4]. In Fig. B3, a slight trend of increasing $T_{e,min}$ with holding time after casting #11 can be seen that could possibly be associated with a slight loss of silicon in the melt. The range of variation of the silicon content during melt holding and of $T_{e,min}$ values with metastable eutectic for each series are reported in Table B1.

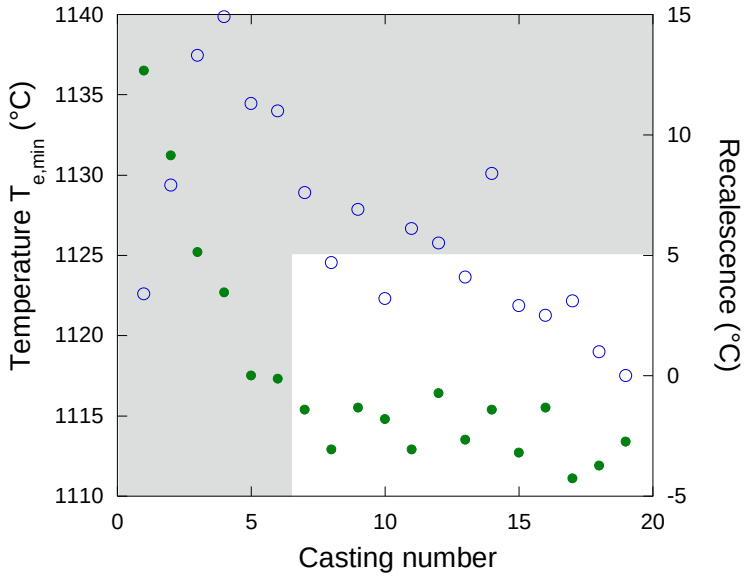

Figure B1. Plot of $T_{e,min}$ (solid symbol) and recalescence (open symbols) for series 1.

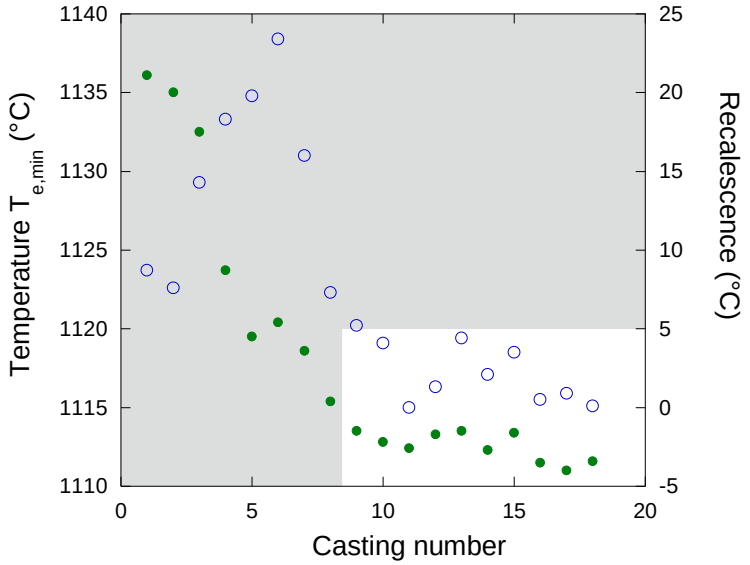

Figure B2. Plot of $T_{e,min}$ (solid symbol) and recalescence (open symbols) for series 2.

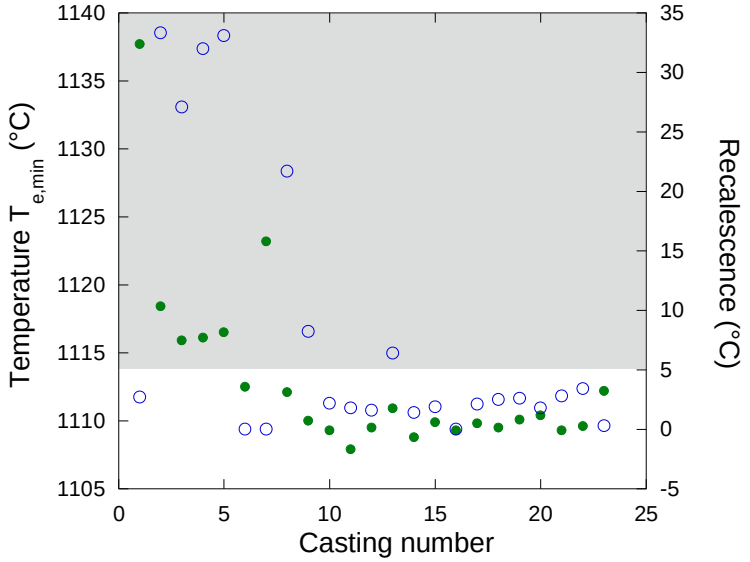

Figure B3. Plot of $T_{e,min}$ (solid symbol) and recalescence (open symbols) for series 4.

Appendix C – Metastable eutectic temperature for cast iron with up to 3.9 wt.% Si

Thermal analysis is regularly performed at the TQC foundry that is associated to Azterlan. During the last decade, some TA records were intended to study solidification in the metastable eutectic. Table C1 lists the composition of the alloys that are referenced as low Si (LoSi) when the Si content is lower than 3 wt.% and high Si (HiSi) otherwise.

All the TA records of these alloys had an arrest at a temperature below 1125°C (see previous section) related to the metastable eutectic, but some did not present a flat part but a continuously decreasing temperature. In this latter case, no $T_{e,min}$ value is reported in Table C-1.

Table C-1. Composition (wt.%) and $T_{e,min}$ values (°C) for LoSi and HiSi alloys

Alloy	%C	%Si	%Mn	**%Cr**	%Mo	%Cu	$T_{e,min}$
LoSi #1	3.51	2.41	0.190	0.040	0.010	0.050	1108.4
LoSi #2	3.45	2.32	0.190	0.040	0.010	0.060	1111.9
LoSi #3	3.67	2.20	0.160	0.030	0.010	0.070	1110.4
HiSi #1	3.16	3.67	0.080	0.040	<0.01	0.020	1084.6
HiSi #2	3.31	3.77	0.065	0.035	0.004	0.024	1087.5
HiSi #3	3.35	3.77	0.079	0.045	0.006	0.029	1082.1
HiSi #4	3.61	3.81	0.066	0.037	0.005	0.024	1080.7
HiSi #5	3.51	3.84	0.180	0.030	0.010	0.070	
HiSi #6	3.22	3.62	0.200	0.040	0.010	0.050	1091.4
HiSi #7	3.25	3.75	0.200	0.030	0.010	0.070	
HiSi #8	3.55	3.48	0.190	0.040	0.010	0.060	1092.9
HiSi #9	3.24	3.73	0.190	0.040	0.010	0.020	
HiSi #10	3.13	3.86	0.200	0.040	0.010	0.020	
HiSi #11	3.05	3.75	0.170	0.040	0.010	0.020	1088.5
HiSi #12	3.03	3.73	0.170	0.040	0.010	0.020	
HiSi #13	3.03	3.72	0.170	0.040	0.010	0.020	